Small-angle multiple scattering of light particles at glancing incidence for screened Coulomb interaction

1992 J. Phys. A: Math. Gen. 25 807

(http://iopscience.iop.org/0305-4470/25/4/019)

J. Phys. A: Math. Gen. 25 (1992) 807–832. Printed in the UK

Small-angle multiple scattering of light particles at glancing incidence for screened Coulomb interaction

K T Waldeer and H M Urbassek

Institut für Theoretische Physik, TU, W-3300 Braunschweig, Federal Republic of Germany

Received 19 February 1991, in final form 7 June 1991

Abstract. We study the multiple scattering process of light particles in random media in the small-angle approximation. Particular consideration is given to the reflection of particles impinging under a glancing angle on a surface. The particle flux is described by a linear integro-differential equation. Results for the space, angle and path-length-dependent particle flux are derived using the method of eigenfunctions. The properties of the solution are discussed for various power-law scattering potentials, and the differences from the well-known diffusion case, corresponding to Coulomb scattering, are emphasized. For the special case of an inverse-square interaction potential, a rigorous solution of the transport equation is derived, and compared to two approximations which have been employed in the literature: deviations occur in particular for small path lengths travelled (small energy loss). The influence of the boundary condition at the surface on the solution is investigated. Applications of the theory to energy loss spectra of reflected particles are discussed.

1. Introduction

If a light-ion beam is injected with a particular direction into a random medium, it is deflected by collisions with target atoms. Whereas wide-angle scattering can be attributed to single scattering events, we shall be concerned with *small-angle scattering*, which stems from the combined effect of many weak scattering events (Bohr 1948, Scott 1963). This so-called multiple scatter process has been investigated theoretically quite intensely in the last two decades (Firsov 1967, 1968, 1970, Sigmund and Winterbon 1974, Marwick and Sigmund 1975, Sigmund *et al* 1978). The restriction to small-angle scattering allows a considerable simplification of the theoretical analysis. When the small-angle approximation holds, a more or less complete solution for the space, angle and path-length-dependent distribution of the scattered particle flux has been found for the case of Coulomb interaction; this solution is commonly called the *diffusion* case (Firsov 1967, 1970, Remizovich 1984). It applies for rather high bombarding energies.

Sometimes, however, multiple scattering of light ions is of interest at lower bombarding energies, when the Coulomb interaction is screened (Mashkova and Molchanov 1985, Hou *et al* 1978, Vukanić and Janev 1986). This is, roughly speaking, the case for light particles, like protons, for energies below some tens of a keV. Here, experiments are performed, where the impinging ion is directed under a glancing angle on a surface (Hou *et al* 1978, Harriss *et al* 1980). These experiments are motivated mainly

0305-4470/92/040807+26$04.50

by the needs of fusion technology for an understanding of light-ion reflection from surfaces. Then most of the reflected particles are again found at glancing emission angle, such that the assumption of small-angle scattering appears justified. In such a case, the multiple scattering distributions are far less completely known. A special case of interest is multiple scattering under an inverse square potential; for this case, only approximate formulae have been derived (Firsov *et al* 1976, Sigmund *et al* 1978), the validity of which is not well known.

Apart from the reflection of light ions form solid surfaces, multiple scattering theory has also been employed for an understanding of energetic electron scattering in solids; here often—but not necessarily (Tilinin 1982)—diffusion theory is adopted (Bethe *et al* 1938, Tolmachev 1986). Scattering of light from atmospheric impurities or local density fluctuations can also be described as a multiple scattering problem (Remizovich *et al* 1981, Gerstl *et al* 1987).

From a mathematical point of view, the solution of the transport equation presents quite a challenging problem. It is an integro-differential equation, differential in the space coordinate and in the path length travelled (usually identified with energy loss), and an integral equation with respect to the angular variables. The mathematical analysis is further complicated by the fact that the integral kernal is strongly polar; this implies that the solution contains generalized functions, or distributions, non-integrable singularities and discontinuities. Examples of these will be found in the formulae below and in several of the graphs. This fact also complicates the analysis on several occasions, for example, where integration and limit operations cannot be interchanged (see appendix 2), or where the straightforward collision number approximation does not converge (section 5.1).

We present in this paper a theoretical study of small-angle multiple scattering processes under glancing incidence, emphasizing the influence of the single scattering potential on the multiple scattering distribution. In particular, we wish to outline the deviations of the distributions under screened Coulomb interaction from the diffusion case. We proceed as follows: the transport equation—a linear integro-differential equation with a strongly singular kernel—and its small-angle approximation are presented in section 2. The general method of solution follows an eigenfunction method (section 3). For multiple scattering distributions in an infinite medium, the general solution is presented as a threefold Fourier integral; all these quadratures can be performed analytically in the diffusion case (section 4). In section 5, we derive a number of special results for the infinite medium case. Among others, a rigorous solution of the multiple scattering problem under inverse square interaction is given (preliminary results have been presented by the authors (1988)), and the behaviour of the distributions for small path lengths is discussed; here drastic quantitative differences appear between the diffusion solution and multiple scattering under screened Coulomb interaction. Since, in experiments, azimuth and polar angle resolved distributions are measured, we present an approximation for the azimuthal part of the distribution and discuss its validity (section 6). In the following section, the influence of the boundary conditions on the scattering distributions is discussed. This is possible analytically by investigating the path length integrated distributions of reflected particles (section 7.1). Furthermore, we present in this section general integral relations which connect infinite medium and half-space distributions. In section 8.1, we compare our analytical result for multiple scattering under an inverse square potential with two approximations which are commonly used in the literature, and discuss the limits of validity of these approximations. As our last issue, we discuss a number of points for the interpretation of the energy

spectra of measured particles and, in particular, the role of straggling in electronic energy loss (section 8.2). An itemized conclusion ends the paper.

2. The transport equation and its small-angle approximation

The theoretical modelling of multiple scattering processes of light particles often resides on a separation of electronic and nuclear stopping events of the projectile in the target. The interaction of the projectile with the target electronic system decelerates the projectile without deflecting it. On the other hand, it can often be assumed that collisions of the light projectile with heavy target atoms lead to only negligible energy loss, but to a definite deflection. Hence, in the common theoretical treatments of multiple scattering, electronic energy loss is neglected at first, and the path-length-dependent multiple scattering distribution due to interaction of the projectile with the screened atomic nuclei is calculated. Electronic energy loss is then re-introduced at a later stage, by convoluting the multiple scatter distribution with an electronic energy loss distribution for given path length (cf section 8.2).

The multiple scatter transport process in random media can be described by a linear Boltzmann equation. Let $f(\boldsymbol{r}, \boldsymbol{\Omega}, E, t)\,\mathrm{d}^3r\,\mathrm{d}E\,\mathrm{d}^2\Omega$ be the mean number of projectiles moving in the target at time t, differential in the position variable $\boldsymbol{r}$, direction of flight $\boldsymbol{\Omega}$ and energy E. It obeys a linear forward Boltzmann equation (Sigmund 1981):

$$\begin{aligned}\frac{\partial}{\partial t}f(\boldsymbol{r},\boldsymbol{\Omega},E,t) + v\boldsymbol{\Omega}\cdot\frac{\partial}{\partial \boldsymbol{r}}f(\boldsymbol{r},\boldsymbol{\Omega},E,t)\\ = N\int \mathrm{d}E\mathrm{d}^2\Omega'\{K(E',\boldsymbol{\Omega}'\to E,\boldsymbol{\Omega})v'f(\boldsymbol{r},\boldsymbol{\Omega}',E',t)\\ - K(E,\boldsymbol{\Omega}\to E',\boldsymbol{\Omega}')vf(\boldsymbol{r},\boldsymbol{\Omega},E,t)\} + \text{sources}. \qquad (1)\end{aligned}$$

Here, v is the velocity of the projectile of energy E, N is the target atom density, and $K(E,\boldsymbol{\Omega}\to E',\boldsymbol{\Omega}')\,\mathrm{d}E'\mathrm{d}^2\Omega'$ is the differential cross section for a particle moving with energy E in direction $\boldsymbol{\Omega}$ to scatter at a resting target atom into energy $(E', \mathrm{d}E')$ and direction $(\boldsymbol{\Omega}', \mathrm{d}^2\Omega')$. It may be written as

$$K(E,\boldsymbol{\Omega}\to E',\boldsymbol{\Omega}')\,\mathrm{d}E'\mathrm{d}^2\Omega' = \frac{1}{2\pi}\delta(\boldsymbol{\Omega}\cdot\boldsymbol{\Omega}'-\hat{\mu})\mathrm{d}^2\Omega'\,\sigma(E,\eta)\mathrm{d}\eta. \qquad (2)$$

Here, $\hat{\mu}$ and η are the direction cosines of the scattering angle in the laboratory system and the centre of mass system, respectively. The energy E' of the scattered particle, and $\hat{\mu}$, can be expressed by η using the laws of kinematics. Finally, $\sigma(E,\eta)$ denotes the scattering cross section.

In the following, we shall be interested in the so-called Lindhard power cross sections, defined by

$$\sigma(E,\eta)\,\mathrm{d}\eta = C\,E^{-2m}(1-\eta)^{-1-m}\,\mathrm{d}\eta \qquad (3)$$

where the power exponent m is in between $0 < m \leq 1$, and the coefficient C is a function of the masses and atomic charges of projectile and target atom (Sigmund 1981). They approximate scattering in inverse power potentials, $V(r) \propto r^{-1/m}$.

Due to the structure of the transport equation (1), it is advantageous to introduce the *flux*

$$\bar{\Phi}(\boldsymbol{r}, \Omega, E, t) = vf(\boldsymbol{r}, \Omega, E, t). \tag{4}$$

We now concentrate on the transport process of very light ions (mass M_p) in a target with mass $M_t \gg M_p$. In this case, particles lose only a negligible amount of energy, and hence we may get rid of the energy variable in equation (1). To this end, we substitute the energy variable by the cosine of the scatter angle η in the centre of mass system. For very light projectiles, the centre of mass system is identical to the laboratory system, i.e. $\eta = \hat{\mu}$; hence integration over the scatter angle in the laboratory system $\hat{\mu}$ is possible. Then we are left with

$$\frac{\partial}{\partial \tau}\bar{\Phi}(\boldsymbol{r}, \Omega, \tau) + \Omega \cdot \frac{\partial}{\partial \boldsymbol{r}}\bar{\Phi}(\boldsymbol{r}, \Omega, \tau)$$
$$= 2^{2m-1}\frac{1-m}{\pi} N\sigma_{tr} \int \mathrm{d}^2\Omega' \frac{\bar{\Phi}(\boldsymbol{r}, \Omega', \tau) - \bar{\Phi}(\boldsymbol{r}, \Omega, \tau)}{|\Omega' - \Omega|^{2+2m}} + \bar{S}(\boldsymbol{r}, \Omega, \tau). \tag{5}$$

Here, $\tau = vt$ measures the path length travelled, and $\bar{S}$ denotes the sources. In addition, σ_{tr} is the transport cross section, defined by

$$\sigma_{tr} = \int_{-1}^{1} \sigma(E, \eta)(1 - \eta)\mathrm{d}\eta. \tag{6}$$

$1/N\sigma_{tr}$ has the intuitive meaning of the length after which a unidirectional beam has become isotropic.

The notation of the angle variables in this paper is taken to apply immediately to the scattering of particles from surfaces under grazing incidence angle. To this end, let the surface be described by the plane $z = 0$ of a cartesian coordinate system, where the z axis is directed perpendicularly into the material. Furthermore, the azimuth angle around the normal is denoted by φ, and the cosine of the polar angle towards the z axis by μ.

In the following we shall not be interested in the lateral spatial variables, so we integrate them out in equation (5), and are left with the flux $\bar{\Phi}(z, \Omega, \tau)$. After scaling all length variables to the mean transport path

$$\Phi(x, \Omega, R) = \frac{1}{N\sigma_{tr}}\bar{\Phi}\left(z = \frac{x}{N\sigma_{tr}}, \Omega, \tau = \frac{R}{N\sigma_{tr}}\right)$$
$$S(x, \Omega, R) = \frac{1}{(N\sigma_{tr})^2}\bar{S}\left(z = \frac{x}{N\sigma_{tr}}, \Omega, \tau = \frac{R}{N\sigma_{tr}}\right) \tag{7}$$

we introduce the small-angle approximation: for a particle entering the medium at a glancing angle with direction cosine $0 < \mu_0 \ll 1$ and initial azimuth angle $\varphi_0 = 0$, for not too large path lengths R, the flux will be centred around $\mu = 0, \varphi = 0$. So the integral limits in equation (5) may be extended to infinity, and we finally obtain

$$\frac{\partial}{\partial R}\Phi(x, \mu, \varphi, R) + \mu\frac{\partial}{\partial x}\Phi(x, \mu, \varphi, R)$$
$$= 2^{2m-1}\frac{1-m}{\pi}\int_{-\infty}^{\infty}\mathrm{d}\varphi' \int_{-\infty}^{\infty}\mathrm{d}\mu' \frac{\Phi(x, \mu', \varphi', R) - \Phi(x, \mu, \varphi, R)}{[(\mu' - \mu)^2 + (\varphi' - \varphi)^2]^{1+m}}$$
$$+ S(x, \mu, \varphi, R). \tag{8}$$

The strongly polar kernel makes the integral divergent for $m \to 1$, as we shall see below. The factor $(1 - m)$ outside the integral sign renders the integration product convergent.

The geometry relevant for equation (8) is sketched in figure 1. Note that μ and μ_0 can also be interpreted as the angle of the projectile flight direction towards the surface; they are positive (negative) for projectiles flying into (out of) the target medium.

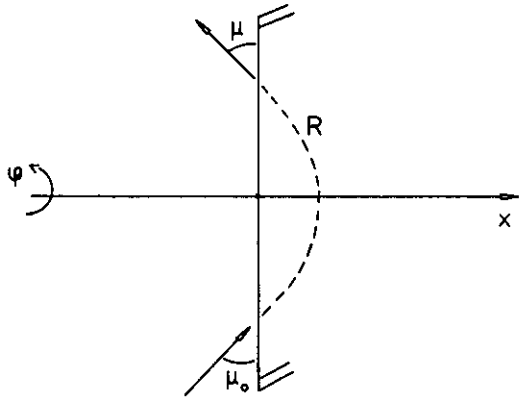

Figure 1. Geometry for glancing angle reflection of light particles from a solid surface. All quantities denoted in scaled form.

Equation (8) is our basic equation. It is a linear integro-differential equation, containing a strongly singular kernel. We shall attempt a solution using the method of eigenfunctions. To make the solution definite we need also boundary and initial conditions, which will be defined below.

3. Solution by eigenfunctions

Let us assume as source one particle entering the medium:

$$S(x, \mu, \varphi, R) = \delta(x)\delta(R)\delta(\mu - \mu_0)\delta(\varphi). \tag{9}$$

Otherwise, at path length $R = 0$, no particle is moving:

$$\Phi(x, \mu, \varphi, R = 0) = 0. \tag{10}$$

This constitutes the initial condition for our equation. With equation (9), the flux is normalized to one:

$$\int_{-\infty}^{\infty} \mathrm{d}x \int_{-\infty}^{\infty} \mathrm{d}\mu \int_{-\infty}^{\infty} \mathrm{d}\varphi \, \Phi(x, \mu, \varphi, R) = 1. \tag{11}$$

Now, the calculation of the general solution of equation (8), with source (9) and initial condition (10), is possible without the need to specify the boundary conditions. This is done by constructing first the general solution of the homogeneous equation (i.e. with source $S \equiv 0$), and second a special solution of the inhomogeneous equation.

After Laplace transformation of equation (8) in R

$$\Phi(x,\mu,\varphi,s) = \int_0^\infty \mathrm{d}R\, \mathrm{e}^{-sR}\Phi(x,\mu,\varphi,R) \tag{12}$$

the general solution of the homogeneous equation with $S = 0$ is given by

$$\Phi_{\mathrm{hom}}(x,\mu,\varphi,s) = \int_{-\infty}^\infty \mathrm{d}\beta \int_{-\infty}^\infty \mathrm{d}\alpha\, A(\alpha,\beta;s)\mathrm{e}^{-x/\alpha} D_m(\mu - \alpha s,\varphi;\alpha,\beta). \tag{13}$$

Here, $D_m(u,v;\xi,\eta)$ is the angular eigenfunction of the linear integro-differential operator in equation (8) with eigenvalues η,ξ and arguments u,v for a fixed value m:

$$D_m(u,v;\xi,\eta) = \left(\frac{1}{\sqrt{2\pi}}\right)^3 \mathrm{e}^{\mathrm{i}\eta v} \int_{-\infty}^\infty \mathrm{d}p \exp\left(\mathrm{i}up + \mathrm{i}\xi\gamma_m \int_0^p \left(\hat{p}^2 + \eta^2\right)^m \mathrm{d}\hat{p}\right)$$

$$\gamma_m = \frac{1-m}{2}\frac{\pi}{\left[\Gamma(m+1)\right]^2 \sin m\pi}. \tag{14}$$

This expression holds true only for $m < 1$. The validity of equation (13) can be proved by inserting it in the Laplace transformed equation (8), using definition (14). The spectral density $A(\alpha,\beta;s)$ still has to be specified by the boundary conditions of the problem.

The angular eigenfunctions $D_m(u,v;\xi,\eta)$ obey the orthogonality relation with weight u:

$$\int_{-\infty}^\infty \mathrm{d}v \int_{-\infty}^\infty \mathrm{d}u\, u\, D_m(u,v;\xi,\eta)\overline{D_m}(u,v;\xi',\eta') = \xi\,\delta(\xi-\xi')\delta(\eta-\eta'). \tag{15}$$

Here $\overline{D_m}$ is the complex conjugate of D_m. Another very important relation we shall use is the expansion of the δ function in angular eigenfunctions:

$$\int_{-\infty}^\infty \mathrm{d}\eta \int_{-\infty}^\infty \frac{\mathrm{d}\xi}{\xi} D_m(u,v;\xi,\eta)\overline{D_m}(u',v';\xi,\eta) = \frac{1}{u}\,\delta(u-u')\,\delta(v-v'). \tag{16}$$

The proof of both relations is straightforward, using definition (14).

To obtain a special solution of the Laplace transformed equation (8), we use the method of variation of constants, which is well known from the theory of linear differential equations. Let the spectral density $A(\alpha,\beta;s)$ be depth dependent in equation (13); after inserting this into equation (8), we derive a differential equation for the x-dependent spectral density. The solution of this equation is inserted into equation (13) and leads to the special solution of the Laplace transformed inhomogeneous equation (8):

$$\Phi_{\mathrm{part}}(x,\mu,\varphi,s;\mu_0)$$

$$= \int_{-\infty}^\infty \mathrm{d}\beta \int_{-\infty}^\infty \frac{\mathrm{d}\alpha}{|\alpha|}\,\theta\left(\frac{x}{\alpha}\right)\mathrm{e}^{-x/\alpha}\overline{D_m}(\mu_0 - \alpha s, 0;\alpha,\beta) \times D_m(\mu - \alpha s,\varphi;\alpha\beta). \tag{17}$$

Here $\theta(\zeta)$ denotes the Heaviside step function. The sum of the general solution of the homogeneous equation and the special solution of the inhomogeneous one,

$$\Phi(x,\mu,\varphi,s;\mu_0) = \Phi_{\text{hom}}(x,\mu,\varphi,s) + \Phi_{\text{part}}(x,\mu,\varphi,s;\mu_0) \tag{18}$$

is after Laplace inversion the general solution of the problem, given by equations (8)–(10). After the specification of boundary conditions, the spectral density $A(\alpha,\beta;s)$ and hence the entire solution can be uniquely determined.

The solution of equation (8) with Coulomb interaction $m = 1$ leads to a different set of eigenfunctions (Remizovich 1984). We were not able to obtain analytical results in this case. In the following, we often use $m = 1$, but in the different meaning of solving equation (8) for all m with the eigenfunctions (14) and then taking the borderline case from the left side $m \to 1^-$. This case is often called the *diffusion solution* (Firsov 1967). Here, the angular eigenfunctions may be expressed by known mathematical functions:

$$D_{m=1}(u,v;\xi,\eta) = \frac{1}{\sqrt{2\pi}}\,\mathrm{e}^{\mathrm{i}\eta v}\left(\frac{2}{|\xi|}\right)^{1/3}\mathrm{Ai}\left[\left(\frac{2}{|\xi|}\right)^{1/3}\left(u-\frac{1}{2}\xi\eta^2\right)\mathrm{sgn}(\eta)\right]. \tag{19}$$

Here, $\mathrm{sgn}(\zeta)$ is the signum function and $\mathrm{Ai}(\zeta)$ is the Airy function using the standard definition (Abramowitz and Stegun 1965).

4. General solution in the infinite medium

In this section we study the solution for infinite medium boundary conditions. Such a medium extends in all directions homogeneously, and the plane $x = 0$ where the projectile enters the medium only acts as a reference plane, and not as a true surface. Obviously, in such a medium, the solution must vanish at large distances from the source:

$$\Phi_{\text{IM}}(|x| \to \infty,\mu,\varphi,R;\mu_0) = 0. \tag{20}$$

Because Φ_{part} vanishes for $|x| \to \infty$, equation (17), and according to equation (13), the spectral density $A(\alpha,\beta;s)$ must be identical to zero, the infinite medium solution is given by the particular solution only,

$$\Phi_{\text{IM}}(x,\mu,\varphi,R;\mu_0) = \Phi_{\text{part}}(x,\mu,\varphi,R;\mu_0). \tag{21}$$

Inserting equation (14) in (17), interchanging integrals and performing the Laplace inversion, we may express Φ_{IM} by the threefold Fourier integral:

$$\begin{aligned}\Phi_{\text{IM}}(x,\mu,\varphi,R;\mu_0) = {} & \left(\frac{1}{2\pi}\right)^3\frac{1}{R} \\ & \times\int_{-\infty}^{\infty}\mathrm{d}p\int_{-\infty}^{\infty}\mathrm{d}p'\int_{-\infty}^{\infty}\mathrm{d}\beta\,\exp\left[\mathrm{i}\left(\mu p+\mu_0 p'+\beta\varphi-\frac{(p'+p)x}{R}\right)\right. \\ & \left.-\gamma_m R\,|\beta|^{2m}\,\frac{I_m(p'/|\beta|)+I_m(p/|\beta|)}{p'+p}\right] \qquad 0<m\le 1\end{aligned} \tag{22}$$

with

$$I_m(y) = \int_0^y (t^2+1)^m \, dt. \tag{23}$$

The infinite medium solution is symmetric in μ and μ_0, and the function $\mu_0^{2m+3}\Phi_{\mathrm{IM}}(x,\mu,\varphi,R;\mu_0)$ depends only on x/μ_0^{2m+1}, R/μ_0^{2m}, μ/μ_0 and φ/μ_0.

The Fourier integrals may be performed explicitly in the diffusion case $m = 1$, and we obtain the well-known result (Rossi and Greisen 1941)

$$\Phi_{\mathrm{IM}}(x,\mu,\varphi,R;\mu_0) = \sqrt{\frac{3}{2}}\frac{1}{\pi^{3/2}}\frac{1}{R^{5/2}} \exp\left\{-\frac{2}{R}\left[\left(\frac{x}{R}-\mu_0\right)^2 + \left(\frac{x}{R}-\mu_0\right)\left(\frac{x}{R}-\mu\right) + \left(\frac{x}{R}-\mu\right)^2 + \frac{\varphi^2}{4}\right]\right\}. \tag{24}$$

We know of no other m value where all three Fourier quadratures can be performed analytically.

5. Results for the infinite medium

In the following, we study special marginal distributions and moments of the flux $\Phi(x,\mu,\varphi,R;\mu_0)$ in order to analyse their characteristic features. The dependence of the flux on the scattering cross section will be of particular interest.

5.1. Behaviour for small R

The distribution for small values of the path length R can be calculated for all values of the power exponent m by expanding equation (8) to first order in the number of collisions occurring. This can be done by adding a small quantity ε in the denominator of the integrand in equation (8). For $R \to 0^+$ and $\varepsilon \to 0$ we then obtain in the small-angle approximation

$$\Phi_{\mathrm{IM}}(x=0,\mu,\varphi,R=0^+;\mu_0) = 2^{2m-1}\frac{1-m}{\pi}\frac{\theta(-\mu)}{[(\mu-\mu_0)^2+\varphi^2]^{1+m}\,|\mu-\mu_0|}. \tag{25}$$

We denote this distribution as the flux of *immediately reflected particles*. One has to bear in mind that the interchange of integration and limit operation $R \to 0^+$ is not rigorously possible. We show in appendix 2 how the generalized functions invoked are dealt with in a mathematically exact way.

For the azimuth integrated flux, the analogous result can be obtained by using a Taylor expansion in equation (22) (cf appendix 2). In equation (25), we clearly see that the diffusion case is atypical, since here $\Phi_{\mathrm{IM}}(R=0^+) \equiv 0$. For all values of $m < 1$, there exists a non-vanishing number of immediately reflected particles. With decreasing value of the power exponent m (more heavily screened Coulomb interaction), the flux of the immediately reflected particles increases and more and more particles are reflected to larger angles $\mu < 0$. This means that the small-angle approximation will become worse for smaller m.

5.2. Azimuth integrated flux

For $m = \frac{1}{2}$ the azimuth integrated flux can be given explicitly (see appendix 1) as

$$\Phi_{\mathrm{IM}}(x,\mu,R,\mu_0) = \frac{\alpha^3}{4\pi^2\mu_0^3}\left(\frac{1+\alpha^2(\gamma-\alpha\beta)(1-\alpha\beta)}{[1+\alpha^2(\gamma-\alpha\beta)^2][1+\alpha^2(1-\alpha\beta)^2]}\right.$$
$$\left. + 2\int_{-1}^{1}\frac{(1+y^2)^2-\alpha^2[(\gamma-1)y+\gamma+1-2\alpha\beta]^2}{\{(1+y^2)^2+\alpha^2[(\gamma-1)y+\gamma+1-2\alpha\beta]^2\}^2}\,\mathrm{d}y\right). \tag{26}$$

Here, the definitions

$$\alpha = \frac{2\mu_0}{R} \qquad \beta = \frac{x}{2\mu_0^2} \qquad \gamma = \frac{\mu}{\mu_0} \tag{27}$$

have been employed. The remaining integration in equation (26) can be performed analytically; the result is given in equation (A1.6) in appendix 1.

Figure 2 displays the azimuth integrated fluxes for $m = \frac{1}{2}$ and 1 at the reference plane $x = 0$ calculated with equations (24) and (A1.6). They are suitably scaled to be universal for all μ_0; thus absolute values are not immediately comparable. In the diffusion case $m = 1$, the main part of the distribution is situated at $\mu < 0$. The maximum in μ is independent of R; it is situated at $\mu/\mu_0 = -\frac{1}{2}$ and the distribution is symmetric with respect to this maximum. For small R, the distribution vanishes exponentially, because all particles leaving the source in direction $\mu_0 > 0$ have to travel a finite path length, before they can invert their direction of flight to $\mu < 0$. For large R, the distribution vanishes as $1/R^2$.

For $m = \frac{1}{2}$, the distribution is also mainly situated at $\mu < 0$. However, for $R = 0$, the maximum is at $\mu = 0$; it changes with increasing R to the asymptotic value $\mu/\mu_0 = -(6\pi+16)/(9\pi+32) \approx -0.5782$. The distribution is rather asymmetric around this maximum, decreasing much faster in the direction of positive μ. The most striking difference from the diffusion case, however, is the existence of a non-vanishing number of particles reflected immediately; cf section 5.1 above. The distribution of these immediately reflected particles at $R = 0^+$ has its maximum at $\mu = 0^-$; it decreases fast with decreasing $\mu < 0$; cf equation (25).

5.3. Flux at $x = 0$

The flux at the reference plane $x = 0$, integrated over R and φ,

$$\Phi_{\mathrm{IM}}(x=0,\mu;\mu_0) = \int_0^\infty \mathrm{d}R \int_{-\infty}^{\infty} \mathrm{d}\varphi\, \Phi_{\mathrm{IM}}(x=0,\mu,\varphi,R;\mu_0) \tag{28}$$

can readily be calculated for $m = \frac{1}{2}$ and $m = 1$:

$$\Phi_{\mathrm{IM}}(x=0,\mu;\mu_0) = \frac{\sqrt{3}}{2\pi}\frac{1}{\mu^2+\mu\mu_0+\mu_0^2} \qquad \text{for } m = 1$$

$$\Phi_{\mathrm{IM}}(x=0,\mu;\mu_0) = \frac{1}{2\pi}\frac{1}{\mu^2+\mu_0^2}\left(1-\frac{4}{\pi}\frac{\mu\mu_0}{\mu^2-\mu_0^2}\log\left|\frac{\mu}{\mu_0}\right|\right) \qquad \text{for } m = \tfrac{1}{2}. \tag{29}$$

The results are displayed in figure 3. They will be discussed jointly with the corresponding half-space distributions in section 7.1.

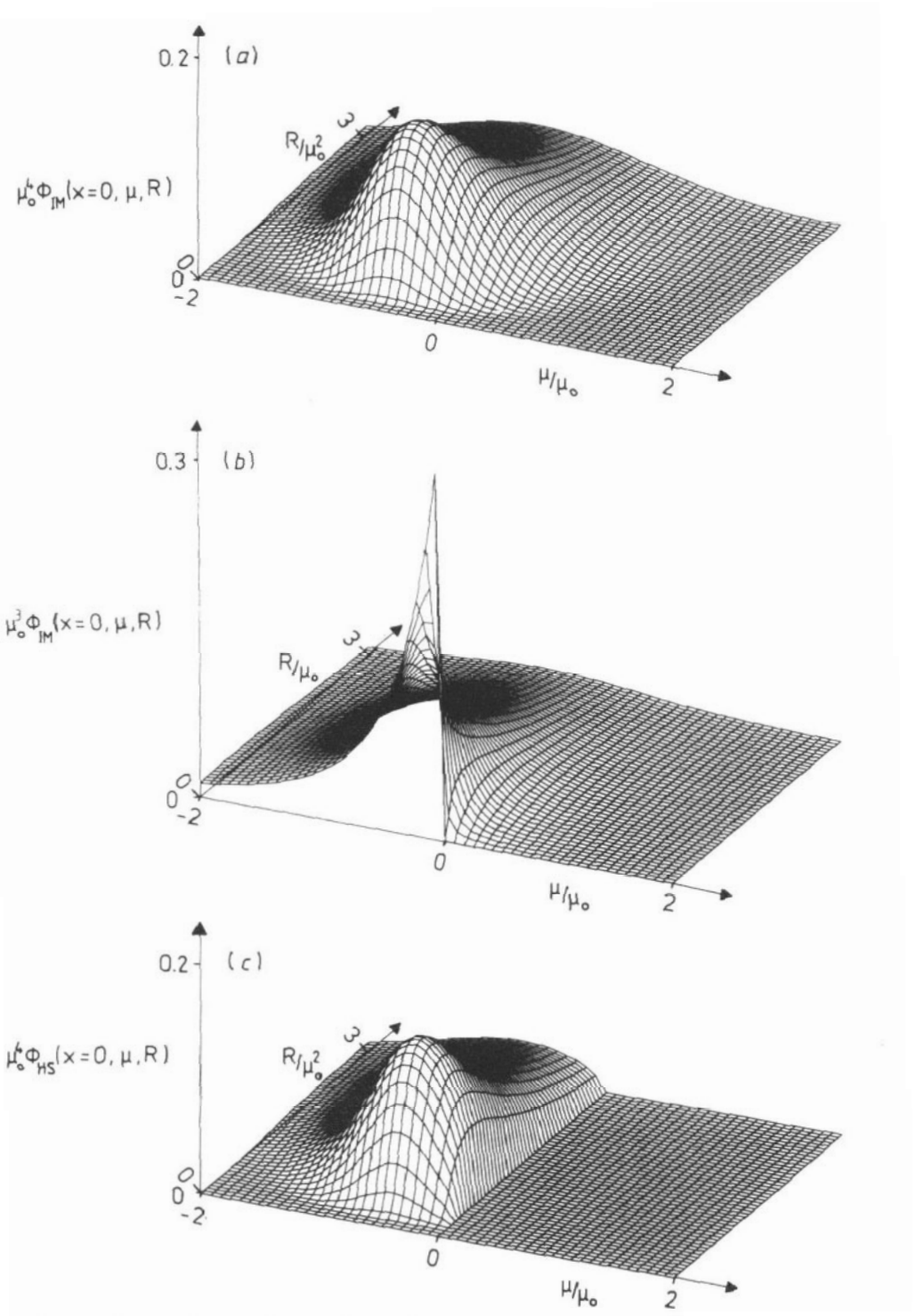

Figure 2. Flux at $x = 0$ for infinite medium and half-space boundary conditions. (*a*) $m = 1$, infinite medium; (*b*) $m = \frac{1}{2}$, infinite medium; (*c*) $m = 1$, half-space.

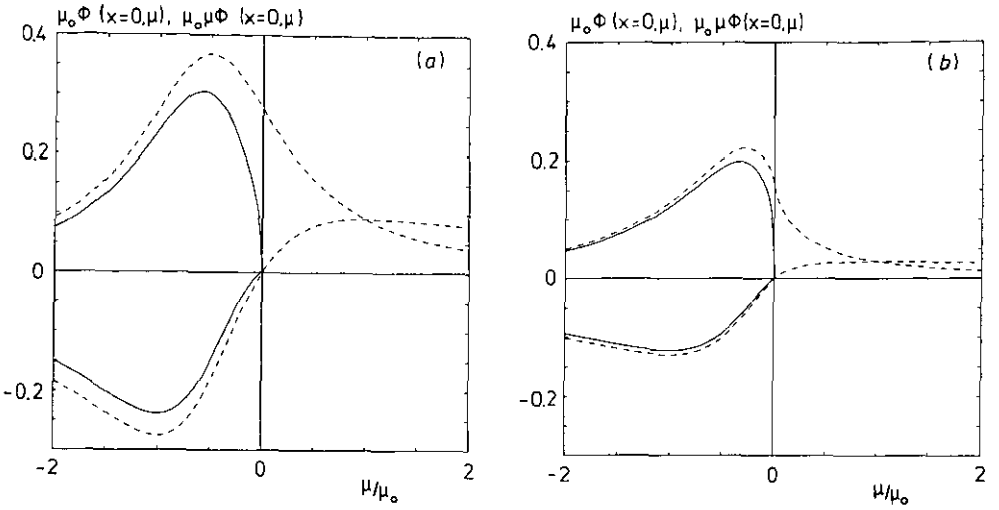

Figure 3. Path-length integrated flux Φ and the particle current density $\mu\Phi$ at $x = 0$ for infinite medium (broken curve) and half-space boundary conditions. (*a*) $m = 1$; (*b*) $m = \frac{1}{2}$.

5.4. Angle integrated flux

The angle integrated flux

$$\Phi_{\mathrm{IM}}(x, R; \mu_0) = \int_{-\infty}^{\infty} \mathrm{d}\varphi \int_{-\infty}^{\infty} \mathrm{d}\mu \, \Phi_{\mathrm{IM}}(x, \mu, \varphi, R; \mu_0) \tag{30}$$

may be calculated for all $m < 1$ as a series expansion in $R/|x/R\mu_0 - 1|^{2m}$ or its inverse:

$$\begin{aligned}\Phi_{\mathrm{IM}}(x, R; \mu_0) &= \frac{2m}{\pi} \frac{1}{\mu_0^{2m+1}} \frac{1}{4m^2} \sum_{n=0}^{\infty} \frac{(-1)^n}{(2n)!} \Gamma\left(\frac{2m+1}{2m}\right) \left(\frac{2m+1}{\gamma_m}\right)^{(2m+1)/2m} \\ &\quad \times \left(\frac{\mu_0^{2m}}{R}\right)^{[2(m+n)+1]/2m} \left|\frac{x}{R\mu_0} - 1\right|^{2n} \\ &= \frac{2m}{\pi} \frac{1}{\mu_0^{2m+1}} \sum_{n=0}^{\infty} \frac{(-1)^n}{n!} \Gamma(2m(n+1)) \sin \pi m(n+1) \left(\frac{\gamma_m}{2m+1}\right)^{n+1} \\ &\quad \times \left(\frac{R}{\mu_0^{2m}}\right)^n \left|\frac{x}{R\mu_0} - 1\right|^{-2m(n+1)-1} . \end{aligned} \tag{31}$$

For special values of m, equation (31) may be expressed by known mathematical functions:

$$\begin{aligned}\Phi_{\mathrm{IM}}(x, R; \mu_0) &= \sqrt{\frac{3}{2\pi}} \frac{1}{R^{3/2}} \exp\left(-\frac{3}{2R^3}(x - \mu_0 R)^2\right) && \text{for } m = 1 \\ \Phi_{\mathrm{IM}}(x, R; \mu_0) &= \frac{2}{\pi} \frac{1}{R^2} \frac{1}{1 + (4/R^4)(x - \mu_0 R)^2} && \text{for } m = \tfrac{1}{2} \\ \Phi_{\mathrm{IM}}(x, R; \mu_0) &= \frac{4\sqrt{\pi}}{\Gamma(1/4)^2} \frac{R^{3/2}}{|x - \mu_0 R|^{3/2}} \, g\left(\frac{4\sqrt{\pi} R}{\Gamma(1/4)^2} \sqrt{\frac{R}{|x - \mu_0 R|}}\right) && \text{for } m = \tfrac{1}{4} \end{aligned} \tag{32}$$

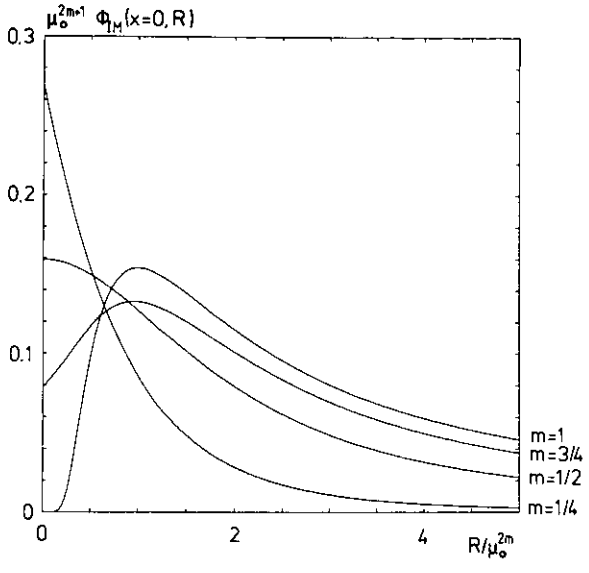

Figure 4. Range distribution of the flux at $x = 0$ for an infinite medium for several values of m.

where $g(\zeta)$ is an auxilary function to the Fresnel integrals using the standard definition (Abramowitz and Stegun 1965).

In figure 4, $\Phi(x = 0, R, \mu_0)\mu_0^{2m+1}$ is plotted against R/μ_0^{2m} for $m = 1$, $\frac{3}{4}$, $\frac{1}{2}$ and $\frac{1}{4}$, using equations (31) and (32). Here, as in figure 2, we observe the flux of the immediately reflected particles for $m < 1$ at $R = 0$. With decreasing m, the maximum of the path length distribution shifts to smaller values of R until, for $m \leq \frac{1}{2}$, it is located at $R = 0$. Corresponding to this enhancement at $R = 0$, the distribution descreases more steeply at large R with decreasing power exponent m. Note that the angle integrated particle current density is given by $\langle\mu\rangle_{x,R}\Phi(x, R; \mu_0)$; here, the brackets denote a moment of the distribution function; cf section 5.5 below. Especially at $x = 0$, it is proportional to Φ. So it has the same dependence on R as Φ.

We note that in the case of isotropic hard sphere scattering (corresponding to $m = -1$ in our notation in equation (5)), the reflected flux can be calculated analytically without introducing any approximations. The immediately reflected flux then is proportional to $|\mu - \mu_0|^{-1}$ (Kuščer and Zweifel 1965).

5.5. Moments

In order to understand the interdependence of flight direction μ, depth x and path length R, we calculate the mean direction of flight $\langle\mu\rangle_{x,R}$ for fixed values of x and R and the mean depth $\langle x\rangle_{\mu,R}$ for fixed values of μ and R after integration over the azimuth angle. Here, the brackets $\langle\ \rangle$ denote moments; e.g. $\langle\mu\rangle_{x,R}$ is defined by

$$\langle\mu\rangle_{x,R} = \frac{\int \mu\Phi(x, \mu, R; \mu_0)\,\mathrm{d}\mu}{\int \Phi(x, \mu, R; \mu_0)\,\mathrm{d}\mu}. \tag{33}$$

From equation (22) we obtain

$$\langle \mu \rangle_{x,R} = \frac{2m+1}{2m}\frac{x}{R} - \frac{1}{2m}\mu_0$$
$$\langle x \rangle_{\mu,R} = \frac{R}{2}(\mu + \mu_0). \tag{34}$$

Thus, for fixed path length R travelled, there is a range of depths x, where the mean direction of flight is positive, i.e. particles continue flying deeper into the medium. But for larger path lengths, the mean direction is inverted. In particular, in the limit $R \to \infty$ or at the surface $x = 0$, the mean direction of the particle current is $\langle \mu \rangle_{x=0,R} = -\mu_0/(2m)$, which is well known (Sigmund *et al* 1978). In the diffusion case, the mean value of the angular distribution at $x = 0$ is identical to the maximum value of $\Phi(x = 0, \mu, R)$ (figure 2(*a*)) for all R, which must obviously be the case for a Gaussian distribution. In the case of $m = \frac{1}{2}$, the angular mean value is $\langle \mu \rangle_{x=0,R} = -\mu_0$, i.e. at the specular angle. This is a larger reflection angle than the maximum value for any path length R (figure 2(*b*)).

The mean penetration depth $\langle x \rangle_{\mu,R}$ is independent of m and proportional to R. It is zero for particles with path length $R = 0$, i.e. particles reflected at once, which is obvious, and for $\mu = -\mu_0$, i.e. for specularly reflected particles. Note that $\langle x \rangle_{\mu,R}$ is independent of the azimuth angle, i.e. $\langle x \rangle_{\mu,R} = \langle x \rangle_{\mu,\varphi,R}$.

6. An approximation for the azimuth dependence

We construct an approximation to the function $I_m(y)$ in equation (22) from its behaviour at small and large values of the argument:

$$I_m(y) = y + \frac{1}{2m+1}|y|^{2m} y. \tag{35}$$

The quality of this approximation can be judged from figure 5, where it is plotted for several values of m. For $m = 1$, it is exact; with decreasing m, the region $y \cong 1$ is less satisfactorily approximated.

Inserting equation (35) in (22), the azimuth integration can be factorized from the remainder:

$$\tilde{\Phi}_{\mathrm{IM}}(x, \mu, \varphi, R; \mu_0) = \Phi_{\mathrm{IM}}(\varphi, R)\, \Phi_{\mathrm{IM}}(x, \mu, R; \mu_0) \tag{36}$$

where

$$\Phi_{\mathrm{IM}}(\varphi, R) = \int_{-\infty}^{\infty} \mathrm{d}x \int_{-\infty}^{\infty} \mathrm{d}\mu\, \Phi_{\mathrm{IM}}(x, \mu, \varphi, R; \mu_0)$$
$$= \frac{1}{\pi}\int_0^{\infty} \mathrm{d}\beta\, \cos(\beta\varphi) \mathrm{e}^{-\gamma_m R \beta^{2m}} \tag{37}$$

and

$$\Phi_{\mathrm{IM}}(x, \mu, R; \mu_0) = \int_{-\infty}^{\infty} \mathrm{d}\varphi\, \Phi_{\mathrm{IM}}(x, \mu, \varphi, R; \mu_0). \tag{38}$$

Here the tilde characterizes the approximated function. This approximation assumes the azimuth and the polar angle part of the distribution to be statistically independent.

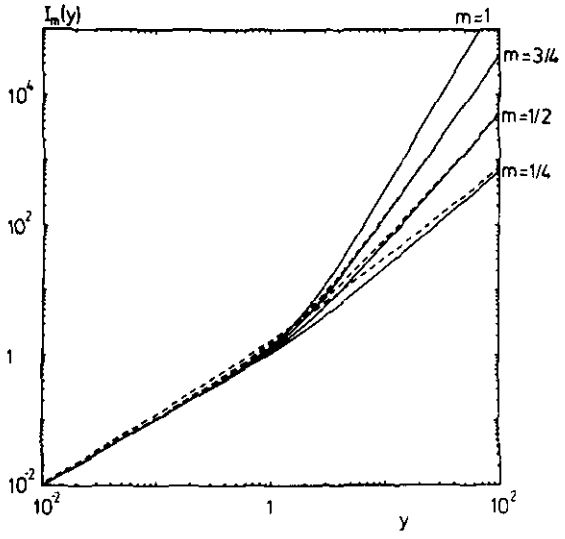

Figure 5. Function $I_m(y)$, equation (22), (full) and its approximation (35) (broken).

It is exact in the diffusion case, where the angular distribution is given as a product of Gaussian distributions. For other values of m, statistical independence no longer holds because, particularly in the immediately backscattered flux, azimuth and polar angle are correlated by the single collision kinematics.

In this approximation, the immediately backscattered flux vanishes for $\varphi \neq 0$, because $\Phi_{\mathrm{IM}}(\varphi, R = 0^+) = \delta(\varphi)$. The azimuth distribution shows a singularity at $\varphi = 0$ for $R \to 0^+$, namely $\Phi_{\mathrm{IM}}(\varphi = 0, R) = \Gamma(1/2m)/2m\pi(\gamma_m R)^{1/2m}$, in contrast to the exact solution (25). Since the influence of $I_m(y)$ on the solution decreases with increasing R very fast, this approximation becomes better for large R.

We study the relative error E of the approximation

$$E = \frac{\Phi(x = 0, \varphi, R; \mu_0) - \tilde{\Phi}(x = 0, \varphi, R; \mu_0)}{\Phi(x = 0, \varphi, R; \mu_0)} \tag{39}$$

in figure 6 for $m = \frac{1}{2}$. In this case,

$$\tilde{\Phi}(x = 0, \varphi, R; \mu_0) = \frac{2}{\pi^2} \frac{R}{(R^2 + \varphi^2)(R^2 + 4\mu_0^2)} \tag{40}$$

whereas $\Phi(x = 0, \varphi, R; \mu_0)$ can be calculated from equation (22) up to one integration, which we performed numerically. We note that for small values of R/μ_0, φ/μ_0 only is the error large. With increasing values, the approximation becomes satisfactory.

7. Half-space

7.1. Flux at the surface

In a half-space problem, no particles can enter the region $x > 0$, with the exception of the projectile at $R = 0$. Thus, the boundary conditions read in this case

$$\begin{aligned} &\Phi_{\mathrm{HS}}(x = 0^-, \mu > 0, \varphi, R; \mu_0) \equiv 0 \\ &\Phi_{\mathrm{HS}}(x \to \infty, \mu, \varphi, R; \mu_0) \cong 0. \end{aligned} \tag{41}$$

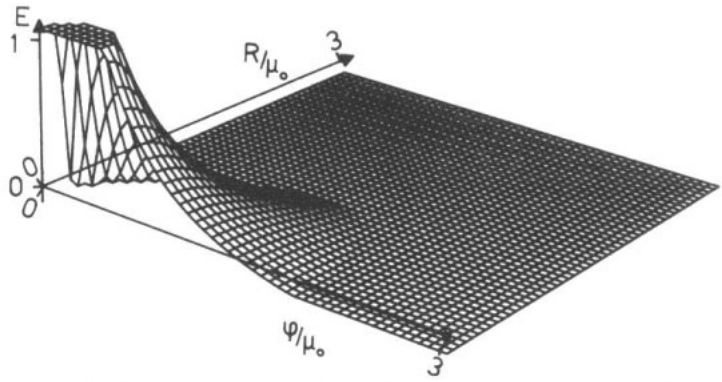

Figure 6. Relative error, equation (39), of the approximation for the azimuth angle resolved flux at $x = 0$ for $m = \frac{1}{2}$.

Let us denote by Φ_0 the—unknown—outgoing flux at the surface

$$\Phi_{\mathrm{HS}}(x = 0^-, \mu < 0, \varphi, R; \mu_0) = \Phi_0(\mu, \phi, R; \mu_0). \tag{42}$$

The problem of determining Φ_{HS} is much more complicated than the infinite medium problem, because the homogeneous part (13) contributes to the general solution, and we need to determine the spectral density $A(\alpha, \beta; s)$. From the boundary condition at infinity, it follows that the spectral density must vanish for $\alpha < 0$. After multiplication of equation (18) with $\mu\overline{D_m}(\mu - \alpha' s, \varphi; \alpha', \beta')$, integrating over μ and φ, using equations (13) and (17), the orthogonality relation (15) and the first boundary condition (41) at the outer surface $x = 0^-$ for $\alpha' < 0$ and all β', we derive an integral equation of the first kind for $\Phi_0(\mu, \varphi, s; \mu_0)$:

$$\int_{-\infty}^{\infty} \mathrm{d}\varphi \int_{-\infty}^{0} \mathrm{d}\mu\, \mu\, \Phi_0(\mu, \varphi, s; \mu_0) D_m(\mu - \alpha' s, \varphi; \alpha', \beta') = -D_m(\mu_0 - \alpha' s, 0; \alpha', \beta') \tag{43}$$

and for $\alpha' > 0$ a reduction formula for the spectral density:

$$\alpha' A(\alpha', \beta'; s) = \int_{-\infty}^{\infty} \mathrm{d}\varphi \int_{-\infty}^{0} \mathrm{d}\mu\, \mu\, \Phi_0(\mu, \varphi, s; \mu_0) \overline{D_m}(\mu - \alpha' s, \varphi; \alpha, \beta'). \tag{44}$$

In order to obtain the solution $\Phi_{\mathrm{HS}}(x, \mu, \varphi, R; \mu_0)$, we first have to determine the flux at the surface using equation (43). Then the spectral density has to be calculated and inserted in equations (13) and (18), and at last a Laplace inversion leads to the general result. Equation (43) is not known to have been solved, but a partial solution is known in the literature (Remizovich 1984).

If one is interested only in the path length and azimuth integrated flux at the surface, $\Phi_0(\mu; \mu_0)$, one may make use of the fact that all particles entering the medium $x \geq 0$ have to leave it again. It can be shown that Φ_0 is a homogeneous function of degree (-2), and equation (43) can be solved using a Mellin transformation in the $(-\alpha')$ variable. Then the result reads for all m (Remizovich 1984):

$$|\mu|\, \Phi_0(\mu; \mu_0) = \frac{1}{\pi \mu_0} \frac{2m+1}{m+1} \sin\left(\pi \frac{m}{m+1}\right) \times \left(\left|\frac{\mu}{\mu_0}\right|^{(2m+1)/(m+1)} + 2\cos\left(\pi \frac{m}{m+1}\right) + \left|\frac{\mu}{\mu_0}\right|^{-(2m+1)/(m+1)} \cdot \right)^{-1}$$
$$\mu < 0 \quad 0 < m \leq 1. \tag{45}$$

In figure 3, the angular distribution of the flux $\Phi_0(\mu, \mu_0)$, and the particle current density $\mu\Phi_0(\mu, \mu_0)$ are plotted for $m = 1$ and $\frac{1}{2}$, using equations (45) and (29). Infinite medium and half-space distributions are displayed. In a half-space, the flux goes to zero at $\mu = 0$. Its maximum lies at smaller $\mu < 0$ for $m = \frac{1}{2}$ than for $m = 1$, although the particle current density at the surface has largest modulus at $\mu = -\mu_0$ and is outward directed. These features hold true for all other values of m as well.

In the infinite medium, the distributions show qualitatively the same behaviour as the half-space distributions at $\mu < 0$. The particle current density is mainly directed outward with its largest modulus at $\mu = -\mu_0$, and the maximum of the inward directed current density is at $\mu = \mu_0$. As discussed above, in the R-dependent case the flux is symmetric for $m = 1$ and asymmetric for $m = \frac{1}{2}$ with respect to its maximum. We note that, for $m = \frac{1}{2}$, there is only a negligible difference between the infinite medium and the half-space solution for the outgoing flux $\mu < 0$.

The influence of the boundary conditions on the particle flux increases with increasing path length R. For $R = 0$, the solution must obviously be independent of the boundary conditions, since no transport could yet occur. For large R, however, a particle can cross the reference plane $x = 0$ in an infinite medium potentially a large number of times, which is impossible in a half-space. On the other hand, we observed that with decreasing m the particle distribution has more and more weight in the region of small values of R. We are hence led to conclude that with decreasing m the influence of the different boundary conditions on the reflected particle flux should decrease as well. This conclusion is substantiated by comparing figures 3(a) and (b), where infinite medium and half-space fluxes ressemble each other more closely for $m = \frac{1}{2}$ than for $m = 1$.

7.2. Integral relations

There are two equivalent integral equations to determine $\Phi_0(\mu, \varphi, s; \mu_0)$ from the infinite medium solution. From equations (18), (20) and (44) the general half-space solution follows as

$$\Phi_{\mathrm{HS}}(x, \mu, \varphi, s; \mu_0) = \int_{-\infty}^{\infty} \mathrm{d}\varphi' \int_{-\infty}^{0} \mathrm{d}\mu'\, \mu'\, \Phi_0(\mu', \varphi', s; \mu_0)\, \Phi_{\mathrm{IM}}(x, \mu, \varphi, s; \mu', \varphi') + \Phi_{\mathrm{IM}}(x, \mu, \varphi, s; \mu_0) \qquad x \geq 0 \tag{46}$$

with the definition $\Phi_{\mathrm{IM}}(x, \mu, \varphi, s; \mu_0, \varphi_0 = 0) = \Phi_{\mathrm{IM}}(x, \mu, \varphi, s; \mu_0)$. Using the fact that

$$\Phi_{\mathrm{IM}}(x = 0^+, \mu, \varphi, s; \mu', \varphi') - \Phi_{\mathrm{IM}}(x = 0^-, \mu, \varphi, s; \mu', \varphi') = \frac{1}{\mu'}\, \delta(\mu - \mu')\delta(\varphi - \varphi') \tag{47}$$

which follows from equations (16) and (17) for $\mu < 0$ at the surface $x = 0^-$, we derive two integral equations with the infinite medium solution as kernel function:

$$\Phi_0(\mu, \varphi, s; \mu_0) = \Phi_{\mathrm{IM}}(x = 0^+, \mu, \varphi, s; \mu_0) + \int_{-\infty}^{\infty} \mathrm{d}\varphi' \int_{-\infty}^{0} \mathrm{d}\mu'\, \mu'\, \Phi_0(\mu', \varphi', s; \mu_0)\, \Phi_{\mathrm{IM}}(x = 0^+, \mu, \varphi, s; \mu', \varphi')$$

$$\int_{-\infty}^{\infty} \mathrm{d}\varphi' \int_{-\infty}^{0} \mathrm{d}\mu'\, \mu'\, \Phi_0(\mu', \varphi', s; \mu_0)\, \Phi_{\mathrm{IM}}(x = 0^-, \mu, \varphi, s; \mu', \varphi') = -\Phi_{\mathrm{IM}}(x = 0^-, \mu, \varphi, s; \mu_0). \tag{48}$$

These integral equations are well known in ion reflection and Green function theory (Firsov *et al* 1976, Bøttiger *et al* 1971). Using equation (47), it is straightforward to show their equivalence. For $m = 1$, the Laplace transformation of the infinite medium solution is possible analytically and after insertion in one of the two equations (48), we derive integral equations, the solution of which can be found in the literature (Remizovich *et al* 1980a, b). So after a Laplace inversion the half-space solution of the flux at the surface $x = 0^-$ is given as

$$\Phi_0(\mu, \varphi, R; \mu_0) = \Phi_{\mathrm{IM}}(x = 0^-, \mu < 0, \varphi, R; \mu_0) \operatorname{erf}\left(\sqrt{\frac{6\mu_0|\mu|}{R}}\right) \qquad \mu < 0 \qquad (49)$$

where $\operatorname{erf}(\zeta)$ is the error function (Abramowitz and Stegun 1965). The azimuth integrated distribution at the surface, $\Phi_0(\mu, R; \mu_0)$, is plotted in figure 2; it is calculated immediately from equation (49). We note that for $|\mu/\mu_0| < R/3\mu_0^2$, the difference beween the infinite medium and the half-space solution is negligible.

8. Discussion

8.1. Approximations for $m = \frac{1}{2}$

Several approximation formulae exist for the infinite medium solution for the multiple scattering distribution under an inverse square scattering potential, $m = \frac{1}{2}$ (Firsov *et al* 1976, Sigmund *et al* 1978). These have been derived from analogy to the diffusion case. In our nomenclature the approximation due to Firsov *et al* reads (Firsov *et al* 1976)

$$\Phi_{\mathrm{IM}}(x = 0, \mu, R; \mu_0) = \frac{\sqrt{3}}{\pi} \frac{1}{[R^2 + 4(\mu^2 + \mu\mu_0 + \mu_0^2)]^{3/2}}. \qquad (50)$$

Another approximation, by Sigmund *et al*, is given by (Sigmund *et al* 1978, Vukanić and Janev 1986)

$$\Phi_{\mathrm{IM}}(x = 0, \mu, R; \mu_0) = \frac{5}{3\pi^2} \frac{R}{[R^2 + 2(\mu_0 - \mu + \frac{5}{3}|\mu_0 + \mu|)^2][R^2 + 2(\mu_0 - \mu - \frac{5}{3}|\mu_0 + \mu|)^2]}. \qquad (51)$$

These approximations are plotted in figure 7. For R not too small, equations (50) and (51) are good approximations to the exact solution (A1.6), which is displayed in figure 2(*b*). However, equation (51) displays a singularity at $R = 0$ and $\mu/\mu_0 = -\frac{1}{2}$. Only at very small R does equation (51) fail, for it vanishes at $R = 0$ almost everywhere.

In contrast to equation (A1.6), both approximations predict the angular maximum to be at $\mu/\mu_0 = -\frac{1}{2}$ for all R. So neither equation (50) nor (51) is able to describe the features of the distribution at very small R although they have been used in this area (Vukanić and Janev 1986). In fact, the single-collision analysis presented above shows that $\Phi(R \to 0^+)$ does not vanish for $m < 1$ in contrast to approximation (51).

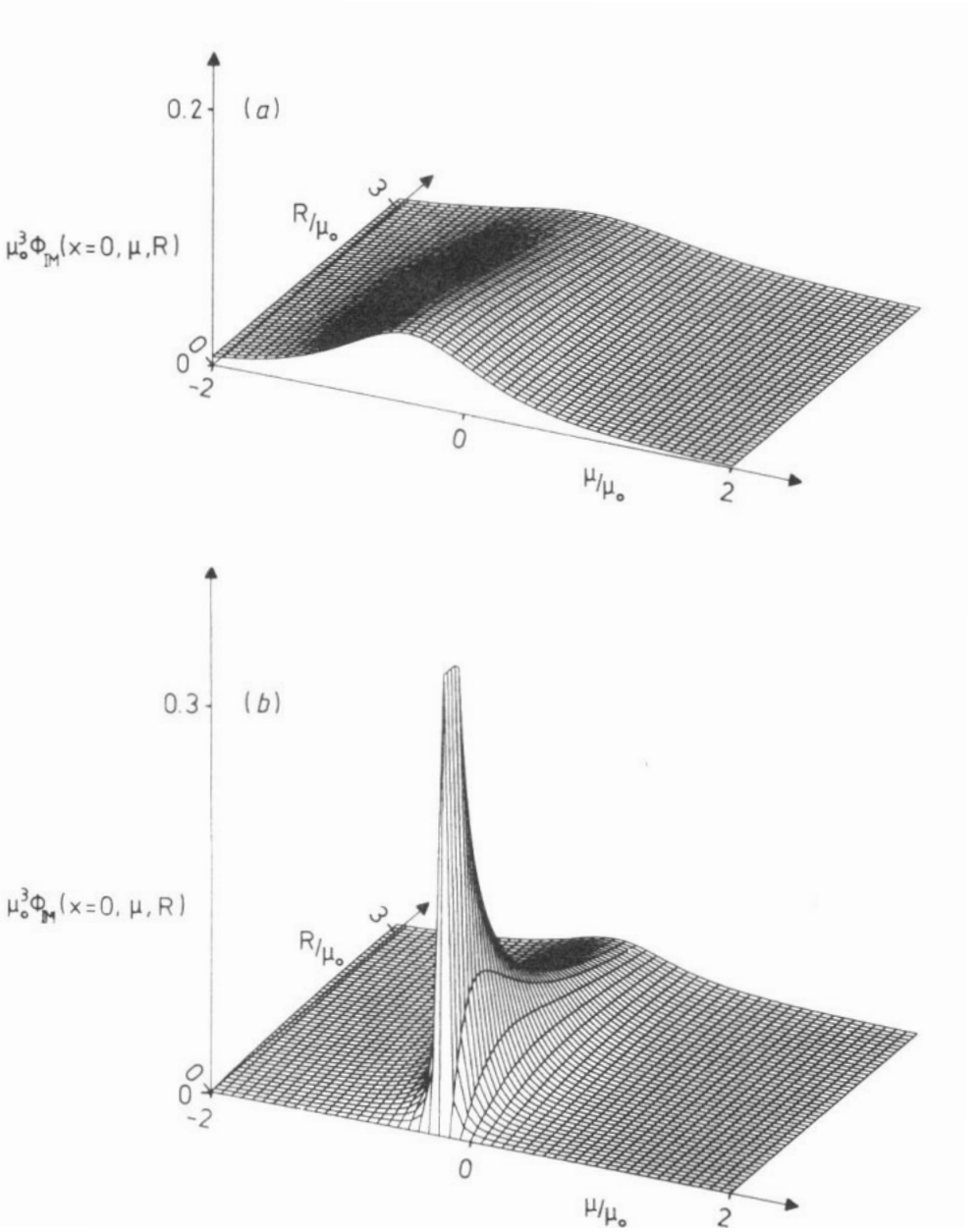

Figure 7. Flux at $x = 0$ for infinite medium boundary condition and $m = \frac{1}{2}$. (*a*) Firsov approximation, equation (50); (*b*) Sigmund approximation, equation (51).

8.2. Energy spectra

For calculating approximate energy spectra of particles, we convolute the angular multiple scattering distribution with an energy loss distribution for given scaled path length R, $F(\epsilon, R)$, i.e.

$$\Phi(x,\mu,\varphi,\epsilon;\mu_0) = \int_0^\infty \mathrm{d}R\, F(\epsilon,R)\Phi(x,\mu,\varphi,R;\mu_0). \tag{52}$$

Here $\hat{\Phi}$ is the flux differential in the energy loss ϵ. There are several possibilities to model the distribution F. For not too large path length τ, the following simple model is often used: τ is set proportional to the energy loss (Vukanić and Janev 1986):

$$\tau = \int_{E_0}^{E} \frac{\mathrm{d}E'}{S_e(E')} \approx \frac{E - E_0}{S_e(E_0)} = \frac{\epsilon}{S_e(E_0)}. \tag{53}$$

Here often only the electronic component S_e of the total stopping power S is considered since it is dominant for the cases of interest here. From the scaling equation (7), we have

$$\tau = \frac{R}{N\sigma_{tr}} = \frac{\gamma E_0}{2} \frac{R}{S_n(E_0)} \tag{54}$$

where $\gamma \simeq 4M_pM_t/(M_p + M_t)^2$ ($\ll 1$). Here we made use of the fact that, for small mass ratios, the transport cross section is proportional to the nuclear stopping power S_n. Then the model assumes that the projectile loses energy at a constant rate, such that path length and energy loss are essentially identical:

$$F(\epsilon, R) = \delta\left(\epsilon - \frac{\gamma E_0}{2} \frac{S_e(E_0)}{S_n(E_0)} R\right). \tag{55}$$

Thus, the path-length-dependent distributions derived in this paper may be immediately interpreted as energy loss spectra.

In order to obtain an idea about the influence of energy straggling, in a first approximation we use a Gaussian energy loss distribution with energy-independent straggling:

$$F(\epsilon, R)\,\mathrm{d}\epsilon = \frac{1}{\sqrt{2\pi\upsilon\omega R}} \exp[-(\epsilon - \upsilon R)^2/2\upsilon\omega R]\,\mathrm{d}\left(\frac{\epsilon}{E_0}\right). \tag{56}$$

Here $\upsilon = \frac{1}{2}\gamma \cdot S_e(E_0)/S_n(E_0)$ and $\omega = W(E_0)/S_e(E_0)E_0$, where $W(E_0) = \int T^2\sigma(E_0, T)\mathrm{d}T$ is the second moment of the collision cross section at the ion impact energy E_0. For light ions of some keV energy, the straggling should be predominantly nuclear. Inserting (56) into (52) in the diffusion case $m = 1$, we obtain the backscattered flux

$$\hat{\Phi}(x = 0, \mu, \varphi, \bar{\epsilon}; \mu_0)$$
$$= \frac{\sqrt{3}}{4\pi^2} \frac{1}{\omega} \sqrt{\frac{\upsilon}{\omega}} \mathrm{e}^{\bar{\epsilon}/\omega} K_2\left[2\sqrt{\frac{\upsilon}{\omega}\left(\mu^2 + \mu\mu_0 + \mu_0^2 + \frac{\varphi^2}{4} + \frac{\bar{\epsilon}}{4\upsilon\omega}\right)}\right]$$
$$\times \left(\mu^2 + \mu\mu_0 + \mu_0^2 + \frac{\varphi^2}{4} + \frac{\bar{\epsilon}}{4\upsilon\omega}\right)^{-1}. \tag{57}$$

Here $\bar{\epsilon} = 1 - E/E_0$ and $K_2(\zeta)$ is the modified Bessel function of second order (Abramowitz and Stegun 1965). In figure 8, equation (57) is plotted for several values of the dimensionless straggling ω. Here, values for forward scattering $\varphi = 0°$, $\mu/\mu_0 = -0.45$ were chosen, and a value of $\upsilon = 0.62$, appropriate for the scattering of 15 keV H^+ from Au in an experiment by Harriss *et al* (1980). With increasing

straggling the distribution broadens and the height of the maximum decreases. For not too large ω, its influence is restricted to high energies, while for higher ω the whole distribution changes without shifting the maximum. There is a small part of the distribution located at energies $E > E_0$. This effect is due to the model of constant energy straggling where the Gaussian distribution F allows particles to gain energy. In a more realistic model this effect should be suppressed by a better choice of F, demanding $\omega = 0$ for $E \geq E_0$. We wish to note that another discussion of the influence of energy straggling on the energy loss distribution of light ions in small-angle multiple scattering theory has been given by Tilinin (1982).

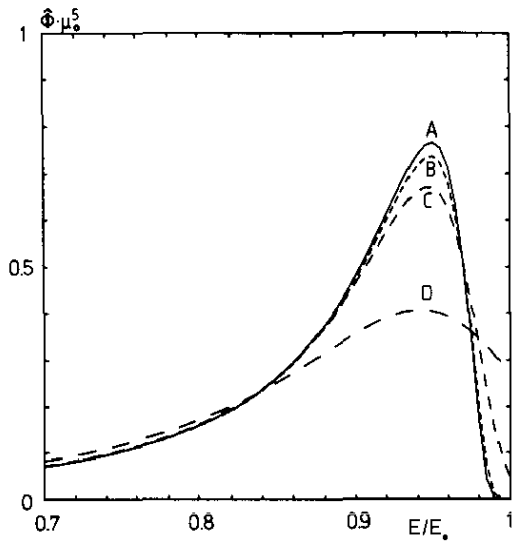

Figure 8. Scaled energy distribution of backscattered particles (equation (57)) for several values of the energy straggling ω. (A) $\omega = 0$, (B) $\omega = 6.7 \times 10^{-4}$, (C) $\omega = 6.7 \times 10^{-3}$, (D) $\omega = 6.7 \times 10^{-2}$.

In figure 9 we compare the results of our theory, equation (22), for $m = \frac{1}{2}$ with experimental data for the specular reflection ($\vartheta = \vartheta_0 = 7.5°$, $\varphi = 0°$) of 5 keV He^+ ions from a polycrystalline Ni surface. In our model, only the parameter $\gamma S_e(E_0)/S_n(E_0)$ enters; it is taken as 0.67 (Vukanić and Janev 1986). For comparison, the azimuth resolved $m = \frac{1}{2}$ approximation (Vukanić and Janev 1986) is also included in the plot. We see that our rigorous solution of the transport equation (8) does not describe the experimental data well for $E \to E_0$. In contrast to the experiment, the transport equation predicts a finite amount of particles to be scattered back with very small energy loss. We ascribe this to the fact that those particles scattered back immediately from the surface (path length $R = 0^+$), do in reality suffer a finite nuclear energy loss in those collisions. This energy loss is not contained in (8). The approximate solution (51) on the other was *forced* to vanish smoothly for $R \to 0^+$: this describes the experimental result better. Summarizing, we wish to conclude that while the overall agreement between the theoretical model, which is without free parameters, and experiment is fair, the quantitative behaviour of the backscattered flux is not predicted as accurately by the model, (8), as one could wish. Finally, we wish to note that in this model *all* particles are eventually reflected out of the target; this is due to the neglect of energy loss in the basic equation (8). Thus we are not able to

obtain accurate reflection coefficients. There do exist recipes in the literature on how to improve on this point (Tilinin 1982).

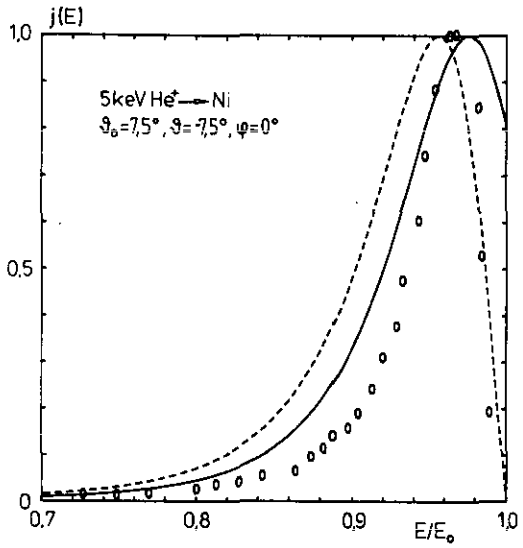

Figure 9. Comparison of experimental data (0) of 5 keV He^+ ions reflected from a Ni surface (Hou *et al* 1978) and theoretical results ($m = \frac{1}{2}$). Incidence angle $\vartheta_0 = 7.5°$, specular scattering conditions. Full line: equation (22); broken line: Vukanić and Janev (1986).

We wish to note that there exist a number of processes not included in the multiple scattering theory that may influence energy spectra. In the theory presented here, the scattering medium has been assumed to be *random*, i.e. structureless. However, already the outermost atom layer at the surface is usually more or less well ordered, and the reflection process may be strongly influenced by processes not treated in our theory. They can usually be verified quite easily from the experimental conditions. We mention three effects which have to be taken into account. If the kinetic energy component of the incoming ion normal to the surface is of the order of the surface binding energy, the backscattering process is evidently determined by the surface and its structure. In this case, the attractive binding interaction of the projectile with the surface also has to be taken into account (Jackson 1980). Second, a particle may be scattered back from the outermost surface layer by the correlated reflection of several surface atoms (*surface channelling*) (Pfandzelter and Schuster 1988). In this case, our transport theory does not apply, since the incoming beam does not really enter the medium. Third, electronic inelastic effects at the surface may dominate the interaction (Närmann *et al* 1990). All these effects gain weight with more glancing incidence angle and smaller bombarding energy. The analysis presented in this paper may be applied to ions which impinge with such a high normal component of the kinetic energy that they can penetrate the surface.

9. Conclusions

(1) The multiple scattering process of light ions is investigated. Special attention is given to the reflection of particles impinging at a glancing angle of incidence on a

surface. Power-law cross sections with power exponent m are employed, and general solutions of the linear integro-differential equation describing the multiple scattering process are obtained using the method of eigenfunctions.

(2) We recover well-known results for the so-called diffusion case, $m = 1$. We give new analytical results for the case of scattering in an inverse square potential, $m = \frac{1}{2}$. Comparison with two approximations used in the literature for this case (Firsov *et al* 1976, Sigmund *et al* 1978) shows deviations in particular at small path lengths or small energy loss.

(3) We investigate the influence of the scattering potential on the small-angle distributions via their dependence on the power exponent m. We find drastic differences for small path lengths R. In the diffusion case, for $R \to 0$, no particles can escape the medium; hence the flux vanishes, $\Phi(R \to 0) \equiv 0$. For $m < 1$, however, there exists a finite probability that particles scatter immediately when entering the medium, and hence $\Phi(R \to 0) > 0$.

(4) For scattering cross sections with $m \leq \frac{1}{2}$, it is most probable that particles leave the medium immediately, i.e. for $R = 0$; this emphasizes the role of single scattering events. For $m > \frac{1}{2}$, on the other hand, particles leave the target most probably after having travelled a finite path length, analogously to the diffusion case.

(5) The influence of the half-space boundary condition on the scattering process is studied. We find that with decreasing value m (i.e. for harder potentials), the angular distributions become more and more similar to scattering distributions in an infinite medium. This is connected to the above mentioned fact that particles most probably travel only short path lengths in the medium. However, for glancing exit angle, the half-space distribution vanishes exactly, unlike the infinite medium solution.

(6) The particle current, integrated over all path lengths, has its maximum at specular reflection for all vallues of the power exponent m. The particle flux shows a more complex behaviour, though: on the average, particles are scattered in the specular direction for an inverse square interaction only. For more (less) heavily screened potentials, particles are reflected at larger (smaller) angles to the surface.

Appendix 1

We present the analytical solution of the azimuth integrated multiple scatter distribution for $m = \frac{1}{2}$. To this end, after azimuth integration, we split in equation (22) the resulting double Fourier transformation into a sum of two double cosine Fourier transformations. One of these may be immediately reduced to a rational function and we are left with

$$\mu_0^3 \Phi_{\mathrm{IM}}(x, \mu, R; \mu_0) = \frac{\alpha^3}{4\pi^2} \left(\frac{1 + \alpha^2(\gamma - \alpha\beta)(1 - \alpha\beta)}{[1 + \alpha^2(\gamma - \alpha\beta)^2][1 + \alpha^2(1 - \alpha\beta)^2]} + \int_0^\infty \int_0^\infty \cos\left(\alpha(\gamma - \alpha\beta)z + \alpha(1 - \alpha\beta)z'\right) \exp\left(-\frac{z'^2 + z^2}{z' + z}\right) \mathrm{d}z \, \mathrm{d}z' \right) \tag{A1.1}$$

with the definitions

$$\alpha = \frac{2\mu_0}{R} \qquad \beta = \frac{x}{2\mu_0^2} \qquad \gamma = \frac{\mu}{\mu_0}. \tag{A1.2}$$

After a rotation of the coordinate system, i.e. $u = z + z'$, $v = z - z'$, the second integral in equation (A1.1) may be expressed as

$$\frac{1}{2}\int_0^\infty \mathrm{d}u\, \mathrm{e}^{-u/2} \int_{-u}^{u} \cos\left(\frac{\alpha}{2}\left[(\gamma + 1 - 2\alpha\beta)u + (\gamma - 1)v\right]\right) \mathrm{e}^{-v^2/(2u)}\mathrm{d}v. \tag{A1.3}$$

Using the substitution $y = v/u$, we interchange the integrals and integrate over u. Thus (A1.3) is reduced to

$$2\int_{-1}^{1} \frac{(1+y^2)^2 - \alpha^2[(\gamma-1)y + \gamma + 1 - 2\alpha\beta]^2}{\{(1+y^2)^2 + \alpha^2[(\gamma-1)y + \gamma + 1 - 2\alpha\beta]^2\}^2}\,\mathrm{d}y. \tag{A1.4}$$

The integrand is a rational function, which is non-singular on the integration path. So a theorem from the calculus of residues may be applied (Behnke and Sommer 1965).

Theorem. If $R(x)$ is a rational function without singularities on its integration path $\mathcal{L}$, the integral is given by

$$\int_{\mathcal{L}} R(z)\,\mathrm{d}z = \sum_{z_k} \frac{1}{(n_k-1)!}\frac{\mathrm{d}^{n_k-1}}{\mathrm{d}z^{n_k-1}}\left[R(z)(z-z_k)^{n_k}\log\frac{z-b}{z-a}\right]\Bigg|_{z=z_k}. \tag{A1.5}$$

Here z_k is the kth pole of order n_k of $R(z)$, a is the start point and b the end point of the integration path $\mathcal{L}$. Since all zeros of the denominator of equation (A1.4) are of second order and two of them are given by equation (A1.7), the other two are their complex conjugates. Operating the above theorem (A1.5) on equation (A1.4) and after some algebraic rearrangement of the terms, we obtain

$$\begin{aligned}\Phi_{\mathrm{IM}}(x,\mu,R;\mu_0) = \frac{2}{\pi^2}\frac{1}{R^3}\Bigg[&\frac{1+(4/R^4)(x-\mu R)(x-\mu_0 R)}{[1+(4/R^4)(x-\mu R)^2][1+(4/R^4)(x-\mu_0 R)^2]}\\
&+ 4\,\mathrm{Re}\Bigg(\frac{1}{(y_1-y_2)^2(y_1-\bar{y}_2)^2(y_1-\bar{y}_1)^2}\Bigg\{4\frac{(1+y_1^2)^2}{y_1^2-1} + \log\left(\frac{y_1-1}{y_1+1}\right)\\
&\times\left[F(y_1) - 4(1+y_1^2)^2\left(\frac{1}{y_1-y_2}+\frac{1}{y_1-\bar{y}_1}+\frac{1}{y_1-\bar{y}_2}\right)\right]\Bigg\}\\
&+\frac{1}{(y_1-y_2)^2(y_2-\bar{y}_1)^2(y_2-\bar{y}_2)^2}\Bigg\{4\frac{(1+y_2^2)^2}{y_2^2-1}+\log\left(\frac{y_2-1}{y_2+1}\right)\\
&\times\left[F(y_2) - 4(1+y_2^2)^2\left(\frac{1}{y_2-y_1}+\frac{1}{y_2-\bar{y}_1}+\frac{1}{y_2-\bar{y}_2}\right)\right]\Bigg\}\Bigg)\Bigg]\end{aligned} \tag{A1.6}$$

with the definitions

$$y_{1/2} = \mathrm{i}\left[-\frac{\mu-\mu_0}{R} \pm \sqrt{\frac{(\mu-\mu_0)^2}{R^2}+1+\mathrm{i}\frac{2}{R}\left(\mu+\mu_0-\frac{x}{R}\right)}\right]$$

$$F(y_k) = 4y_k(1+y_k^2) - 4\frac{\mu-\mu_0}{R^2}\left((\mu-\mu_0)y_k + \mu + \mu_0 - 2\frac{x}{R}\right) \qquad k = 1,2. \tag{A1.7}$$

$\mathrm{Re}(\xi)$ denotes the real part of the complex number ξ and $\bar{y}_k$ the conjugate complex of y_k.

The solution (A1.6) consists of two parts, a rational function and a complicated combination of transcendental functions. They have different physical meaning. If we integrate equation (A1.1) over all μ, the second part of the solution vanishes, as can be shown from equation (A1.4). So equation (32) is generated exclusively by the rational part of the solution (A1.6). On the other hand, if we are interested in the limiting case $R \to 0$, the rational function in equation (A1.6) vanishes, and only the second part of the solution leads after some ponderous calculations with equation (A1.4) to equation (25) for $m = \frac{1}{2}$.

In order to obtain equation (29) for $m = \frac{1}{2}$, we insert equation (A1.1) with the integral representation (A1.4) in equation (28) and integrate over $\xi = \alpha^2$. Thus we derive

$$\begin{aligned}\Phi_{\mathrm{IM}}(x=0,\mu)\mu_0^2 &= \frac{1}{4\pi^2}\left[2\left(\frac{1+\log 2}{\gamma}+\frac{\pi}{\gamma^2+1}-\frac{\gamma+1}{\gamma-1}\frac{2\log|\gamma|}{\gamma^2+1}\right)\right.\\ &+\lim_{\xi\to\infty}\left(\frac{\log(\gamma^2\xi+1)}{\gamma(\gamma+1)}+\frac{\log(\xi+1)}{\gamma+1}\right.\\ &\left.\left.-2\int_{-1}^{1}\frac{\log\{(1+y^2)^2+\xi[(\gamma-1)y+\gamma+1]^2\}}{[(\gamma-1)y+\gamma+1]^2}\,\mathrm{d}y\right)\right]. \qquad \text{(A1.8)}\end{aligned}$$

The limiting case $\xi \to \infty$ is calculated by considering the three logarithmic terms jointly, and then interchanging the limit and the integration. Thus we obtain for the limit

$$\frac{2\log|\gamma|}{\gamma(\gamma+1)}-4\int_{-1}^{1}\frac{\log|[(\gamma-1)y+\gamma+1]|}{[(\gamma-1)y+\gamma+1]^2}\,\mathrm{d}y. \qquad \text{(A1.9)}$$

After solving the integral (A1.9), substituting back into equation (A1.8), and making use of equation (A1.2), we obtain equation (29).

Appendix 2

In order to obtain the azimuth integrated equation (25), we expand the exponential function in equation (22) at $x = 0$ in powers of R. Bearing in mind that $\mu_0 > 0$, for $R = 0^+$ we are left with

$$\begin{aligned}\Phi_{\mathrm{IM}}(x=0,\mu,R=0^+;\mu_0) &= -\frac{1}{4\pi^2}\frac{\gamma_m}{2m+1}\int_{-\infty}^{\infty}\int_{-\infty}^{\infty}\mathrm{e}^{\mathrm{i}\mu p}\mathrm{e}^{-\mathrm{i}\mu_0 p'}\left(p'|p'|^{2m}-p|p|^{2m}\right)\frac{\mathrm{d}p'\mathrm{d}p}{p'-p}\\ &0<m\le 1. \qquad \text{(A2.1)}\end{aligned}$$

With the substitution $p' = z + p$, one integration is partially possible and equation (A2.1) is reduced to

$$\Phi_{\mathrm{IM}}(x=0,\mu,R=0^+;\mu_0) = -\frac{1}{4\pi^2}\frac{\gamma_m}{2m+1}\left(\int_{-\infty}^{\infty} \mathrm{e}^{-\mathrm{i}\mu_0 z}\frac{1}{z}\int_{-\infty}^{\infty} \mathrm{e}^{\mathrm{i}(\mu-\mu_0)p}p|p+z|^{2m}\,\mathrm{d}p\,\mathrm{d}z - 4\pi\sin(m\pi)\Gamma(2m+1)\frac{\delta(\mu)}{|\mu_0|^{2m+1}} + \mathrm{i}\pi\int_{-\infty}^{\infty}\mathrm{e}^{\mathrm{i}(\mu-\mu_0)p}p|p|^{2m}\,\mathrm{d}p\right). \quad \text{(A2.2)}$$

Using the integrals

$$\int_{-\infty}^{\infty}\mathrm{e}^{\mathrm{i}(\mu-\mu_0)p}p|p|^{2m}\,\mathrm{d}p = -2\mathrm{i}\sin(m\pi)\Gamma(2m+2)\frac{\mathrm{sgn}(\mu-\mu_0)}{|\mu-\mu_0|^{2m+1}} \quad \text{(A2.3)}$$

$$\int_{-\infty}^{\infty}\mathrm{e}^{-\mathrm{i}\mu_0 z}\frac{1}{z}\int_{-\infty}^{\infty}\mathrm{e}^{\mathrm{i}(\mu-\mu_0)p}p|p+z|^{2m}\,\mathrm{d}p\,\mathrm{d}z = 2\pi\sin(m\pi)\frac{\Gamma(2m+2)}{|\mu-\mu_0|^{2m+1}}\left(\frac{\mathrm{sgn}(-\mu)}{\mu-\mu_0}+\frac{2}{2m+1}\delta(\mu)\right) \quad \text{(A2.4)}$$

and after some rearrangement of terms in equation (A2.2), we obtain

$$\Phi_{\mathrm{IM}}(x=0,\mu,R=0^+;\mu_0) = \frac{1-m}{m}\frac{\Gamma(2m)}{[\Gamma(m)]^2}\frac{\theta(-\mu)}{|\mu-\mu_0|^{2+2m}}. \quad \text{(A2.5)}$$

This result can be derived as well by integrating equation (25) over φ.

References

Abramowitz M and Stegun I A (eds) 1965 *Handbook of Mathematical Functions* (New York: Dover)

Behnke H and Sommer F 1965 *Theorie der analytischen Funktionen einer komplexen Veränderlichen* (Berlin: Springer)

Bethe H A, Rose M E and Smith L P 1938 *Proc. Am. Phil. Soc.* **78** 573

Bøttiger J, Davies J A, Sigmund P and Winterbon K B 1971 *Radiat. Eff.* **11** 69

Bohr N 1948 *Mat. Fys. Medd. Dansk. Vid. Selsk.* **18** no 8

Firsov O B 1967 *Sov. Phys.-Dokl.* **11** 732

—— 1968 *Sov. Phys.-Solid State* **9** 1687

—— 1970 *Sov. Phys.-Tech. Phys.* **15** 57

Firsov O B, Mashkova E S, Molchanov V A and Snisar V A 1976 *Nucl. Instrum. Methods* **132** 695

Gerstl S A W, Zardecki A, Unruh W P, Stupin D M, Stokes G H and Elliot N 1987 *Appl. Opt.* **26** 779

Harriss J E, Young R and Thomas E W 1980 *J. Appl. Phys.* **51** 5344

Hou M, Eckstein W and Verbeek H 1978 *Radiat. Eff.* **39** 107

Jackson D P 1980 *Radiat. Eff.* **49** 233

Kuščer I and Zweifel P F 1965 *J. Math. Phys.* **6** 1125

Marwick A D and Sigmund P 1975 *Nucl. Instrum. Methods* **126** 317

Mashkova E S and Molchanov V A 1985 *Medium Energy Ion Reflection from Solids* (Amsterdam: North Holland)

Närmann A, Monreal R, Echenique P M, Flores F, Heiland W and Schubert S 1990 *Phys. Rev. Lett.* **64** 1601

Pfandzelter R and Schuster M 1988 *Nucl. Instum. Methods* B **33** 898

Remizovich V S 1984 *Sov. Phys.-JETP* **60** 290
Remizovich V S, Ryazanov M I and Tilinin I S 1980a *Sov. Phys.-JETP* **52** 225
—— 1980b *Sov. Phys.-Dokl.* **25** 272
—— 1981 *Izv. Atmosph. Oceanic Phys.* **17** 654
Rossi B and Greisen K 1941 *Rev. Mod. Phys.* **13** 240
Scott W T 1963 *Rev. Mod. Phys.* **35** 231
Sigmund P 1981 *Sputtering by Particle Bombardment* vol I, ed R Behrisch (Berlin: Springer) p 9
Sigmund P, Heinemeier J, Besenbacher F, Hvelplund P and Knudsen H 1978 *Nucl. Instrum. Methods* **150** 221
Sigmund P and Winterbon K B 1974 *Nucl. Instrum. Methods* **119** 541
Tilinin I S 1982 *Sov. Phys.-JETP* **55** 751
Tolmachev A I 1986 *Sov. Phys.-Tech. Phys.* **31** 760
Vukanić J V and Janev R K 1986 *Nucl. Instrum. Methods* B **16** 22
Waldeer K T and Urbassek H M 1988 *Proc. XIV SPIG '88, Sarajevo* ed N Konjević, L Tanović and N Tanović, contributed papers, p 189